

TESTING OF TURBULENT SEALS FOR ROTORDYNAMIC COEFFICIENTS*

Dara W. Childs and John B. Dressman
Mechanical Engineering Dept.
The University of Louisville
Louisville, Kentucky 40208

S. Bart Childs
Industrial Engineering Dept.
Texas A&M University
College Station, Texas 77840

SUMMARY

A facility has been developed for dynamic testing of straight and convergent-tapered seals, with the capability of separately determining both direct and cross-coupled stiffness, damping, and added mass coefficients. The test apparatus causes the seal journal to execute small-eccentricity centered circular orbits within its bearings. Dynamic measurements are made and recorded of the seal-displacement-vector components, and of the pressure field. The pressure field is integrated to yield seal reaction-force components. The displacement and force vector components are analyzed via a generalized Newton-Raphson procedure to yield the desired seal dynamic coefficients. Representative test data are provided and discussed.

INTRODUCTION

Black [1, 2, 3, 4] in a series of publications incorporating theoretical and experimental results has demonstrated that the rotordynamic behavior of pumps is critically dependent on forces developed by neck-rings and interstage seals illustrated in figure 1. Subsequent experience [5] has demonstrated that the stability of cryogenic turbopumps is comparably dependent on seal forces. The test program discussed here was stimulated by stability difficulties encountered in developing the turbopump of [5], and has the objective of separately identifying stiffness, damping, and inertia coefficients for turbulent seals.

The contents of this section are provided to briefly review theoretical models and prior experimental results and procedures for seals. Also, since the seals of figure 1 are geometrically similar to plain journal bearings, applicable prior test programs to identify journal bearing coefficients are also reviewed.

*The work reported herein was supported by NASA Lewis under NASA Grant 3200; technical monitor Dr. Robert C. Hendricks.

Seal Analysis: Leakage and Dynamic Coefficients

Black [1, 2, 3, 4] is largely responsible for developing currently employed dynamic seal models. Black's analysis yields a definition of the force acting on a rotor due to its motion at a seal location, and is based on the following leakage relationship from Yamada [6] for flow between concentric rotating cylinders.

$$\Delta P = (1 + \xi + 2\sigma)\rho V^2/2 \quad (1)$$

where ξ is a constant entry-loss coefficient, ρ is the fluid density, V is the average fluid velocity, and σ is a friction-loss coefficient defined by

$$\sigma = \bar{\lambda}L/C \quad (2)$$

In the above, L is the seal length, C is the radial clearance, and $\bar{\lambda}$ has been defined by Yamada to be the following function of the axial and radial Reynolds numbers (R_a , R_r)

$$\bar{\lambda} = 0.079 R_a^{-1/4} \left[1 + \left(\frac{7R_r}{8R_a} \right)^2 \right]^{3/8} ; R_a = 2VC/\nu, R_r = R\omega C/\nu \quad (3)$$

where ν is the fluid's kinematic viscosity, R is the seal radius, and ω is the rotor's rotational speed. The friction law definition of Eq. (3), Yamada's definition for $\bar{\lambda}$, is based on an assumed 1/7 power velocity distribution, and fits the Blasius equation for pipe friction.

Black's analysis for a plain non-serrated seal yields a motion/reaction-force definition of the form

$$-\frac{\bar{\lambda}}{R\pi\Delta P} \begin{Bmatrix} R \\ R_Y \end{Bmatrix} \begin{Bmatrix} X \\ Y \end{Bmatrix} = \begin{bmatrix} \tilde{K} & \tilde{k} \\ -\tilde{k} & \tilde{K} \end{bmatrix} \begin{Bmatrix} r_X \\ r_Y \end{Bmatrix} + \begin{bmatrix} \tilde{C} & \tilde{c} \\ -\tilde{c} & \tilde{C} \end{bmatrix} \begin{Bmatrix} \dot{r}_X \\ \dot{r}_Y \end{Bmatrix} + \begin{bmatrix} \tilde{m} & \tilde{o} \\ \tilde{o} & \tilde{m} \end{bmatrix} \begin{Bmatrix} \ddot{r}_X \\ \ddot{r}_Y \end{Bmatrix} \quad (4)$$

where

$$\tilde{K} = \bar{\mu}_0 - \bar{\mu}_2\omega^2T^2/4, \tilde{k} = \bar{\mu}_1\omega T/2, \tilde{C} = \bar{\mu}_1T, \tilde{c} = \bar{\mu}_2\omega T^2, \tilde{m} = \bar{\mu}_2T^2, T = L/V \quad (5)$$

In Black's original analysis [1], the coefficients $\bar{\mu}_0$, $\bar{\mu}_1$, $\bar{\mu}_2$ were developed for short seals for which, "circumferential pressure-induced flows are negligible compared with axial flows". Black subsequently [2] examined

the effect of circumferential pressure-induced flow for finite-length seals, and developed the following formulae to account for finite (L/R) ratios

$$\left. \begin{aligned} \mu_0\left(\frac{L}{R}\right) &= \bar{\mu}_0 \{1 + 0.28(L/R)^2\}^{-1} \\ \mu_1\left(\frac{L}{R}\right) &= \bar{\mu}_1 \{1 + 0.23(L/R)^2\}^{-1} \\ \mu_2\left(\frac{L}{R}\right) &= \bar{\mu}_2 \{1 + 0.06(L/R)^2\}^{-1} \end{aligned} \right\} \quad (6)$$

Black's second refinement of the original development [3] was the definition of $\bar{\mu}_0$, $\bar{\mu}_1$, $\bar{\mu}_2$ in terms of the following additional parameter

$$\beta = \left(\frac{7R_r}{8R_a}\right)^2 / \left\{1 + \left(\frac{7R_r}{8R_a}\right)^2\right\} \quad (7)$$

which accounts for a circumferential variation in $\bar{\lambda}$ due to a radial displacement perturbation from a centered position. Plots of $\bar{\mu}_0$, $\bar{\mu}_1$, and $\bar{\mu}_2$ are provided in figure 2 as a function of β and σ for $\xi = 0.5$. These coefficients are comparatively insensitive to anticipated variations of the entrance loss factor ξ .

Finally, Black [4] examined the influence of inlet swirl on seal coefficients. Specifically, in previous analyses, a fluid element entering a seal was assumed to instantaneously achieve the half-speed tangential velocity $R\omega/2$. Black in [4] demonstrates that a fluid element must travel a substantial distance axially along the seal before asymptotically approaching this limiting velocity. The practical consequence of this swirl effect is that predictions for the cross-coupling terms \tilde{k} , \tilde{c} may be substantially reduced.

One of the authors [7] has recently completed a seal analysis based on Hirs turbulent lubrication model [8,9], which largely repeats Black's developments (which were based on various ad hoc models). The results resemble, but do not coincide with Black's results. They also do not include the finite-length correction of Eq. (6).

Prior Seal Testing Procedures and Results

The pertinent data which must be measured to confirm the seal leakage model of Eqs. (1) - (3) are ΔP , V (from flow rate), ω , and the axial pressure gradient within the seal. This latter measurement yields σ which in turn yields $\bar{\lambda}$. Yamada's model for the friction factor was based on testing for these variables over the Reynolds number range ($200 \leq R_a \leq 40,000$; $0 \leq R_r \leq 40,000$) and clearance to radius ratios of ($.0106 \leq C/R \leq .0129$).

Various approaches can be taken to the measurement of seal dynamic properties as defined by Eqs. (4) and (5). For example, if the journal segment

of the seal is stationary (i.e., $\dot{r}_X = \dot{r}_Y = \ddot{r}_X = \ddot{r}_Y = 0$), Eq. (4) can be inverted to obtain

$$\begin{Bmatrix} r_X \\ r_Y \end{Bmatrix} = - \frac{\bar{\lambda}}{R\pi PK_e^2} \begin{bmatrix} \tilde{K} & -\tilde{k} \\ \tilde{k} & \tilde{K} \end{bmatrix} \begin{Bmatrix} R_X \\ R_Y \end{Bmatrix}, K_e^2 = \tilde{K}^2 + \tilde{k}^2$$

Hence by applying the static load definition ($F_X = F_S, F_Y = 0$), and measuring the displacement components r_X, r_Y , one obtains a combined measure of the direct and cross-coupled stiffness coefficients. This is predominantly the type of testing performed by Black, who cites results in the form of "receptance magnitudes", i.e.,

$$|r|/F_S = \bar{\lambda} \{ \tilde{K}^2 + \tilde{k}^2 \}^{1/2} / R\pi\Delta P$$

From Black's model, the relative magnitudes of the direct \tilde{K} and cross-coupled \tilde{k} stiffness coefficients depend on the relative magnitudes of the axial and radial Reynolds numbers. Specifically, at zero running speeds \tilde{k} is zero, but increases with R_r , and can exceed \tilde{K} .

For softly supported rotors, the direct stiffness of a non-serrated seal represented by \tilde{K} may significantly influence the location of a critical speed. However, the stability of a flexible rotor is less sensitive to the direct stiffness term, depending primarily on the cross-coupled stiffness coefficient \tilde{k} , and direct damping coefficient \tilde{C} . For most rotors, the cross-coupled damping coefficients \tilde{c} , and inertia terms \tilde{m} have no appreciable influence on rotor stability or response.

Most of Black's testing [2, 3, 10, 11] has been of the static nature cited above. The second type of test cited consists of analytically modeling a test rotor including the theoretically predicted seal dynamics, and comparing the dynamic characteristics of the model with test data. For example, in [2] the test rotor was rapped and a correlation was made with the observed logarithmic decrement on the decay curve. In [3], known imbalances were applied to the test rotor, and a comparison was made with synchronous amplitudes and phase, critical-speed location, and onset speed of instability. Comparisons between rotor model results and tests, of this nature, are helpful in deciding whether the general seal model is reasonable. However, this type of test-correlation does not yield specific information about the individual dynamic coefficients. Further, discrepancies between predictions and results can be the result of either an inadequate rotor model or an inadequate seal model. For example, in [3], Black indicates that discrepancies in synchronous amplitude and phase results could result from an inadequate initial balance.

A summary of the test results of references [2, 3, 10, 11] is provided in Table 1. The correlation in these tests ranges from "good" to "fair". The nature and results of the test support the following general conclusions

concerning the adequacy of Black's dynamic seal model:

- (a) Over the Reynolds number range tested, the prediction of the direct stiffness coefficient \tilde{K} is adequate for plain and serrated seals, although less accurate for serrated seals. Black's test results indicate a divergence between tests and theory for the direct damping coefficient \tilde{C} as the axial Reynolds number is increased.
- (b) Although the data cited generally supports Black's dynamic seal model over the Reynolds number range considered, it is inadequate to specifically verify the proposed relationships [Eq. (5)] for the dynamic coefficients as functions of the axial and radial Reynolds numbers.

Identification of the dynamic coefficients of seals in a centered position as functions of the axial and radial Reynolds numbers is the objective of the current test program.

Prior Journal-Bearing Coefficient Identification Approaches

The seals of figure 1 are geometrically similar to plain journal bearings but have larger C/R ratios on the order of 0.01 as compared to bearings for which C/R is on the order of 0.001. Seals customarily operate in the turbulent regime, both axially and circumferentially, and have a substantial direct stiffness at a centered zero eccentricity position. Further, seals are nominally designed to operate in a centered position, while the operating eccentricities of journal bearings vary with running speed and load. Hence, dynamic bearing-identification work has generally had the objective of validating dynamic coefficients versus eccentricity relationships. The general similarities between bearings and seals are such that procedures developed for bearing-coefficient-identification may also apply for seals and are briefly reviewed below.

On the basis of various analyses, the motion/reaction-force relationship for a hydrodynamic bearing is defined, for small motion about an equilibrium position, by the equation

$$\begin{bmatrix} C_{xx} & C_{xy} \\ C_{yx} & C_{yy} \end{bmatrix} \begin{Bmatrix} \dot{r}_X \\ \dot{r}_Y \end{Bmatrix} + \begin{bmatrix} K_{xx} & K_{xy} \\ K_{yx} & K_{yy} \end{bmatrix} \begin{Bmatrix} r_X \\ r_Y \end{Bmatrix} = - \begin{Bmatrix} R_X \\ R_Y \end{Bmatrix} \quad (8)$$

The equations of motion of a rigid rotor of mass $2M$ supported symmetrically by two identical bearings can then be stated

$$\begin{bmatrix} M & 0 \\ 0 & M \end{bmatrix} \begin{Bmatrix} \ddot{r}_x \\ \ddot{r}_y \end{Bmatrix} + \begin{bmatrix} C_{xx} & C_{xy} \\ C_{yx} & C_{yy} \end{bmatrix} \begin{Bmatrix} \dot{r}_x \\ \dot{r}_y \end{Bmatrix} + \begin{bmatrix} K_{xx} & K_{xy} \\ K_{yx} & K_{yy} \end{bmatrix} \begin{Bmatrix} r_x \\ r_y \end{Bmatrix} = M\omega^2 a \begin{Bmatrix} \cos(\omega t) \\ \sin(\omega t) \end{Bmatrix} + \begin{Bmatrix} F_X \\ F_Y \end{Bmatrix} \quad (9)$$

Where F_x , F_y are the components of the external force vector, a is the imbalance vector magnitude and ω is the constant rotor spin speed.

Published work related to the identification of the stiffness and damping coefficients of Eq. (9) date from Gleinecke [12] who excited the bearing segment of a 120 mm model bearing in two mutually orthogonal directions while measuring the amplitude and phase of the relative motion between the bearing and journal. The stiffness and damping coefficients are calculated from the frequency-domain equations. Morton [13] adopted this test procedure on a full-scale 308 mm (20 in.) industrial bearing, to calculate bearing stiffness and damping coefficients, and subsequently [14] developed a technique for introducing a step input into a full-scale operating turbine bearing, thereby defining the bearing transfer function. Burrows and Stanway [15] have proposed the use of a pseudo-random-binary sequence (pros) excitation force with a multiple-regression analysis for estimating the coefficients. Their estimation procedure consists of the following steps:

- (a) The governing differential equations of motion (2) are expressed in state-variable format, i.e., as a system of first-order differential equations.
- (b) The first-order differential equations are replaced by first-order difference equations.
- (c) The unknown coefficients are calculated based on a minimum error-squared criterion from measurements of the state variables and the pros input signal.

They also applied the method to the estimation of squeeze-film damper coefficients [16].

THE UNIVERSITY OF LOUISVILLE DYNAMIC SEAL TEST PROGRAM

Test Section Design

Figure 3 illustrates the test-section design employed in the current seal test program. Water enters the center of the section and flows axially across the two rotating test seals exiting at the bottom of the test section. The seal journals ($L = 4$ in = 10.16 cm, $D = 2$ in = 5.08 cm) are mounted eccentrically on the shaft with a constant eccentricity $e_s = .005$ in = 1.27×10^{-4} m. The nominal seal clearance is $C = .02$ in = 5.08 mm, which yields $C/R = .01$. Accordingly, shaft rotation causes the seal journals to execute circular centered orbits at the nominal eccentricity ratio $\epsilon = 0.25$. Axial and radial Reynolds numbers may be specified over the range $Re_a \in [5000, 30,000]$ $Re_r \in [0, 11,000]$ by varying the shaft rotational speed (0 - 4,000 rpm) and flow-rate. Shaft-speed is measured by a once-per-revolution counter, while turbine flowmeters separately measure flowrate through each seal.

The rotor of figure 3 is supported in Torrington hollow roller

bearings¹ [17]. These precision bearings are preloaded radially, have zero internal clearances, and an accurately predictable radial stiffness. When supported in these bearings, the stiff rotor design of figure 3 yields a first critical speed of approximately 12,500 rpm. The end thrust bearing is provided to react the small axial load developed by the opposed test-seal design.

Instrumentation and Data Analysis

The dynamic instrumentation illustrated in figures 3 and 4 consists, for each seal, of Bently eddy-current motion transducers and five piezo-electric pressure transducers which are distributed both axially and circumferentially along and around the seal. The circumferential "clocking" of the pressure transducers is provided primarily as a matter of convenience, since the transducers are provided exclusively to define the time history of the axial pressure distribution. Since the seal journal is forced to execute a closed circular orbit at constant speed ω within its journal, the steady-state pressure distribution is constant with respect to an observer fixed to the shaft, and the circumferential pressure distribution at time \bar{t} , $p(z, \theta)$ is definable in terms of either past or future time measurements $p(z, t)$ at a fixed value of θ .

The direct extraction of circumferential pressure distributions from pressure time histories also permits the "reconstruction" of a pressure time history at a given circumferential location (e.g., $\theta = 0$), despite the fact that the transducers are distributed circumferentially around the seal as illustrated in figure 4. Specifically, given the measurements $p_1(t)$, $p_2(t)$, ... $p_5(t)$, the corresponding pressure signals for $\theta = 0$ are

$$\left. \begin{aligned} p_1^*(t) &= p_1(t) \\ p_2^*(t) &= p_2(t + \bar{\beta}/\omega) \\ \dots\dots\dots \\ p_5^*(t) &= p_5(t + 4\bar{\beta}/\omega) \end{aligned} \right\} \quad (10)$$

where ω is again the shaft rotational speed. In words, the pressure measurements $p_i^*(\bar{t})$ define the axial pressure distribution at time $t = \bar{t}$ for $\theta = 0$.

The seal reaction forces at a given time $t = \bar{t}$ are defined by the integrals

¹These bearings were donated by Torrington through the kindness of W. L. Bowen, whose assistance is gratefully acknowledged.

$$R_x(\bar{t}) = - \int_0^{2\pi} \int_0^L p(\theta, z) \sin\theta R d\theta dz$$

$$R_y(\bar{t}) = - \int_0^{2\pi} \int_0^L p(\theta, z) \cos\theta R d\theta dz$$
(11)

with θ as illustrated in figure 4. These integrals may also be stated as

$$R_X(\bar{t}) = -RL \int_0^{2\pi} \sin\theta \bar{p}(\theta) d\theta = -R\omega L \int_0^{\frac{2\pi}{\omega}} \sin\omega\tau \bar{p}(\tau) d\tau$$

$$R_Y(\bar{t}) = -RL \int_0^{2\pi} \cos\theta \bar{p}(\theta) d\theta = -R\omega L \int_0^{\frac{2\pi}{\omega}} \cos\omega\tau \bar{p}(\tau) d\tau$$
(12)

where \bar{p} is the average axial pressure defined by

$$\bar{p}(\theta) = \frac{1}{L} \int_0^L p(\theta, z) dz, \quad \bar{p}(t) = \frac{1}{L} \int_0^L p(t, z) dz$$
(13)

The integral of Eq. (13) is evaluated numerically from the pressure time histories $p_i^*(t)$. The axial spacing of the pressure transducers has been chosen from Gauss-Legendre quadrature formulas [18] to minimize the error involved in evaluating this integral, and yields the following simple formula for the integration with respect to z

$$\bar{p}(t) = \frac{1}{2} \{ A_1 p_1^*(t) + A_2 p_2^*(t) + A_3 p_3^*(t) + A_2 p_4^*(t) + A_1 p_5^*(t) \}$$

where

$$A_1 = 0.23693, \quad A_2 = 0.47862, \quad A_3 = 0.56889$$

The time integrals in Eq. (12) are executed with a simple Simpson's-rule-based algorithm. Note that a pressure time-history is required over the interval $[\bar{t}, \bar{t} + 2\pi/\omega]$ to obtain $R_X(\bar{t}), R_Y(\bar{t})$. Hence, pressure time histories $p_i^*(t)$ over a total time period ΔT will yield force histories $R_X(t), R_Y(t)$ over the reduced interval $[\Delta T - 2\pi/\omega]$. However, since the signals are periodic, an

adequate sampling rate² yields sufficient output ($r_X(t)$, $r_Y(t)$, $R_X(t)$, $R_Y(t)$) from a limited number of data cycles to identify the dynamic seal coefficients K , k , C , c , m of the following dimensional version of Eq. (4)

$$\begin{bmatrix} m & 0 \\ 0 & m \end{bmatrix} \begin{Bmatrix} \ddot{r}_X \\ \ddot{r}_Y \end{Bmatrix} + \begin{bmatrix} C & c \\ -c & C \end{bmatrix} \begin{Bmatrix} \dot{r}_X \\ \dot{r}_Y \end{Bmatrix} + \begin{bmatrix} K & k \\ -k & K \end{bmatrix} \begin{Bmatrix} r_X \\ r_Y \end{Bmatrix} = - \begin{Bmatrix} R_X \\ R_Y \end{Bmatrix} \quad (14)$$

Note that m in this equation is the seal added fluid mass, and has nothing to do with the actual mass of the test rotor. Eq. (14) is solely the seal governing equation, and the test procedure which yields $r_X(t)$, $r_Y(t)$, $R_X(t)$, $R_Y(t)$ is not influenced by dynamics of the test-section rotor.

Identification Procedure

A generalized NR (Newton-Raphson) procedure [19], [20], [21] is employed for parameter identification. This procedure can be visualized as fitting the solution of Eqs. (14) to the observed data, in much the same manner regression analysis does with algebraic models. These solutions are obtained by numerical integration of the ordinary differential Eqs. (14). Note that this procedure operates on the differential Eq. (14), and is not a frequency-response or transfer-function approach. In fact, a frequency-response approach can provide only a restricted amount of information from the circular-orbit data of this program. This statement is illustrated by substituting the assumed solution

$$r_X = A \cos \omega t, \quad r_Y = A \sin \omega t$$

into Eq. (14), solving for (R_X, R_Y) , and forming the dot and cross products

$$\frac{|r_X R|}{A^2} = k - C\omega, \quad \frac{r \cdot R}{A^2} = m\omega^2 - c\omega - K$$

For a given speed ω , a frequency-response approach yields the sums on the right hand side of these expressions; however, the N-R procedure can separately identify the coefficients.

The N-R procedure as applied to Eq. (14) requires the following first-order restatement

²Biomation data acquisition units are employed with a sampling rate per channel of 100,000 Hz to digitally record $r_X(t)$, $r_Y(t)$ and $p_i(t)$.

$$\left. \begin{aligned}
 \dot{y}_1 &= y_3 \\
 \dot{y}_2 &= y_4 \\
 \dot{y}_3 &= -y_5 y_3 - y_6 y_4 - y_7 y_1 - y_8 y_2 + y_9 f_1(t) \\
 \dot{y}_4 &= +y_6 y_3 - y_5 y_4 + y_8 y_1 - y_7 y_2 + y_9 f_2(t) \\
 \dot{y}_5 &= \dot{y}_6 = \dot{y}_7 = \dot{y}_8 = \dot{y}_9 = 0
 \end{aligned} \right\} \quad (15)$$

The identities relating Eqs. (14) and (15) are $y_1 = \dot{r}_X$, $y_2 = \dot{r}_Y$, $y_3 = r_X$, $y_4 = r_Y$, $y_5 = C/m$, $y_6 = c/m$, $y_7 = K/m$, $y_8 = k/m$, and $y_9 = 1/m$. Note that the original differential equations have been augmented by the trivial differential equations, $\dot{m} = 0$, $\dot{K} = 0$, etc., to enforce the time invariance of these seal coefficients. The identification procedure minimizes, in a least-square sense, the errors between the solution to Eq. (15) and the test data.

Unfortunately, this procedure involves the solution of a multipoint-boundary value problem for which existence and uniqueness theorems are simply not available. Hence, the procedure was validated [21] by generating fake data with simulated noise and theoretically predicted seal coefficients, and then analyzing the data to "identify" the coefficients. Even with severely degraded data, the procedure yields errors less than 8%.

TEST RESULTS AND DISCUSSION

Experimental Results

The beginning phase of testing has consisted of marginal advances followed by precipitous retreats. Tests were conducted on straight seals ($D = 4$ in, $L/D = 0.5$, $C/R = 0.01$) in June and October 1979. Because of data transfer problems, the bulk of the dynamic data taken in June was unusable; however, test results for three good R_a , R_r sets are provided in the first three rows of Table 2. These data sets indicate that experimental estimates of m , C , c , k are smaller than predicted, while K is substantially larger. Figure 5(a) illustrates the theoretical [7] and experimental pressure distributions for case 1 of Table 2, demonstrating that the experimental pressure amplitudes are smaller than predicted. The oscillation observable in P_3 of this figure is exactly 18 times rotational speed (3660 rpm), and is at present unexplained. However, as illustrated in figure 6(a), the integration which yields the force components eliminates this and all other fourier components, leaving only the fundamental component of running speed. The displacement vector components are illustrated in figure 6(b). The "notch" in the lower portion of these signals is the result of damage to the seal journal extension caused by rubbing of the displacement transducer probe during start up.

Tests in October 1979 were repeated in the straight seal configuration; however, the measured pressure fields were noisy and erratic, and one of the pressure transducers failed. When the test unit was disassembled, chemical deposits were found on the seal bearing and journal. These deposits apparently formed when the test section was drained following the June test series. The deposits were irregular, and substantially increased the surface roughness of the seals. The results of two tests from this series are provided in the last two rows of Table 2, demonstrating the same basic trend as the June tests. Note, however, that the added mass term is now larger than predicted.

The leakage $-\Delta P$ data for a large number of tests has consistently deviated from Black's and Yamada's results in that the leakage is consistently (by 5 to 8%) smaller than predicted.

Discussion of Results

Generally speaking, an inadequate amount of data has been taken to support any conclusions about the adequacy of the theory. The differences between the tests in June and October are consistent with the theory in that an increase in surface roughness would increase σ . Over the range of σ anticipated, the coefficient μ_2 is much more sensitive to σ than μ_0 , μ_1 . Hence, a relatively sharper increase in the added mass m is anticipated with increasing surface roughness.

The reduced leakage results obtained in the tests as compared to Yamada's and Black's predictions are at present unexplained. It is possible that the oscillating entry clearance accounts for this result.

Additional Planned Testing

Tests were conducted on a seal with a convergent tapered sleeve segment during April 1980, and the dynamic data related to this test are currently being processed and analyzed. The taper angle for the seal tested is less than optimal [22] from a direct stiffness viewpoint. Tests will also be conducted on both an optimal taper seal and a seal with a taper angle approximately 25% larger than optimal.

Tests will be repeated in June of 1980 on the straight seal over a wide Reynolds number range. The straight seal will then be modified by rounding the sleeve inlet.

Strain-gauge pressure transducers are on order to replace and/or complement the piezo-electric transducers presently employed. With these new transducers, we should get a better idea of the dynamic entry loss, and dynamic pressure gradient.

REFERENCES

1. Black, H. F., "Effects of Hydraulic Forces in Annular Pressure Seals on the Vibrations of Centrifugal Pump Rotors," J. M.Eng. Sci., Vol. 11, No. 2, pp. 206-213, 1969.
2. Black, H. F. and Jensen, D. N., "Dynamic Hybrid Properties of Annular Pressure Seals," Proc. J. Mech. Engin., Vol. 184, pp. 92-100, 1970.
3. Black, H. F. and Jensen, D. N., "Effects of High Pressure Ring Seals on Pump Rotor Vibrations," ASME Paper No. 71-WA/FF-38, 1971.
4. Black, H. F., "The Effect of Inlet Flow Swirl on the Dynamic Coefficients of High-Pressure Annular Clearance Seals," unpublished analyses performed at the University of Virginia, Charlottesville, Va., August 1977.
5. Childs, D., "The Space Shuttle Main Engine High-Pressure Fuel Turbopump Rotordynamic Instability Problem," ASME Transactions for Power, pp. 48-57, January 1978.
6. Yamada, Y., "Resistance of Flow through Annulus with an Inner Rotating Cylinder," Bul. J.S.M.E., Vol. 5, No. 18, pp. 302-310, 1962.
7. Childs, D. W., "Dynamic Analysis of Turbulent Annular Seals Based on Hirs' Lubrication Equation," submitted to ASME Trans., J. of Lubrication Technology.
8. Hirs, G. G., "Fundamentals of a Bulk-Flow Theory for Turbulent Lubricant Films," Doctoral Thesis, Delft Technical University, Delft, The Netherlands, June 1970.
9. Hirs, G. G., "A Bulk-Flow Theory for Turbulence in Lubricant Films," ASME J. Lubrication Technology, pp. 137-146, April 1973.
10. Black, H. F., "Empirical Treatment of Hydrodynamic Journal Bearing Performance in the Superlaminar Regime," J. Mech. Engin. Sci., Vol. 12, No. 2, pp. 116-122, 1970.
11. Black, H. F. and Cochrane, E. A., "Leakage and Hybrid Bearing Properties of Serrated Seals in Centrifugal Pumps," Paper G5, 6th International Conference on Fluid Sealing, February 27 - March 2, 1973, Munich, German Federal Republic.
12. Glienecke, J., "Experimental Investigation of the Stiffness and Damping Coefficients of Turbine Bearings and Their Application to Instability Prediction," Proceedings of the Institute of Mechanical Engineers, Vol. 181, Series 88, p. 116, 1966-67.
13. Morton, P. G., "Measurement of the Dynamic Characteristics of a Large Sleeve Bearing," ASME Trans., Journal of Lubrication Technology, pp. 143-150, January 1971.

14. Morton, P. G., "The Derivation of Bearing Characteristics by Means of Transient Excitation Applied Directly to a Rotating Shaft," G.E.C. Journal of Science and Technology, Vol. 42, pp. 43-47, 1975.
15. Burrows, C. R. and Stanway, R., "Identification of Journal Bearing Characteristics," ASME Trans., Journal of Dynamic Systems, Measurement and Control, pp. 167-173, September 1977.
16. Stanway, R., Burrows, C. R., and Holmes, R., "Parametric Excitation of a Squeeze-Film Bearing," 5th IFAC Symposium on Identification and Parameter Estimation, September 24-28, 1979.
17. Bowen, W. L. and Bhateja, "The Hollow Roller Bearing," ASME Paper No. 79-Lub-15, ASME-ASLE Lubrication Conference, Dayton, Ohio, October 16-18, 1979.
18. Fröberg, Introduction to Numerical Analysis, Second Edition, Addison Wesley, 1969.
19. Childs, B., Luckinbill, D., Bryan, J., and Boyd, J., "Numerical Solution of Multipoint Boundary Value Problems in Linear Systems," Int. J. Systems Science, pp. 49-57, 2(1971).
20. Childs, B., Doiron, H., and Holloway, C., "Numerical Solution of Multipoint Boundary Value Problems in Nonlinear Systems," Int. J. Systems Science, pp. 53-66, 2(1971).
21. Childs, B., Childs, D., and Dressman, J., "Estimation of Seal Stiffness and Damping Parameters from Experimental Data," accepted for presentation at the 2nd International Conference on Vibrations in Rotating Machinery, Cambridge, England, September 2-4, 1980.
22. Fleming, D. P., "High-Stiffness Seals for Rotor Critical-Speed Control," ASME Paper No. 77-DE7-10, Design Engineering Technical Conference, Chicago, Illinois, 26-30 September 1977.

Ref.	R_a	R_r	L/D	(C/R) x 10	Seal Type	Cited Results
[2]	[6,000, 14,000]	[0, 3,500]	.25 , .5, 1.	10.5 , 12.9	plain	a, b, c
[3]	[3,000, 20,000]	[0, 6,000]	.5, 1.	7.23, 10.3	plain	d, e
[10]	10,000	[0, 8,000]	1.	10.7	plain	f
[11]	[3,000, 12,000]	[0, 6,000]	.232, .5, 1.	7.1	Serrated	d

- a. Static force-deflection curves for $0 \leq \epsilon \leq 0.8$.
- b. Resultant stiffness F_s/r for centered position and $\omega = 0$.
- c. Rotordynamic modeling to correlate with test data on the direct damping coefficient \tilde{c} .
- d. Receptance magnitudes for centered position.
- e. Rotordynamic modeling to correlate with synchronous test results. Correlation includes amplitude, phase, critical speed, and onset speed of instability.
- f. Receptance magnitude and phase at centered position.

TABLE 1. PRIOR DYNAMIC SEAL TESTS

		C	c	K	k	m	
1.	$R_a = 18,317$	Theory	47.	14.	9712	3585	0.06
	$R_r = 10,079$	Estimated	21.	2.5	14170	2700	0.013
2.	$R_a = 11,997$	Theory	31.	14.	4592	3046	0.06
	$R_r = 10,410$	Estimated	22.	0.33	8859	3204	0.017
3.	$R_a = 20,814$	Theory	53.4	14.	12203	3879	0.06
	$R_r = 10,079$	Estimated	25.9	2.89	16972	2556	0.013
4.	$R_a = 17,834$	Theory	50.2	4.0	9106	855	0.07
	$R_r = 2,644$	Estimated	13.2	14.3	9662	655	0.098
5.	$R_a = 19,022$	Theory	54.0	8.9	10739	2096	0.07
	$R_r = 5,783$	Estimated	18.6	1.33	14759	2200	0.113

Table 2. Test Results for June 1979 (Rows 1, 2, 3) and October 1979 (Columns 4, 5) versus Theory [7] (in-lb-sec units)

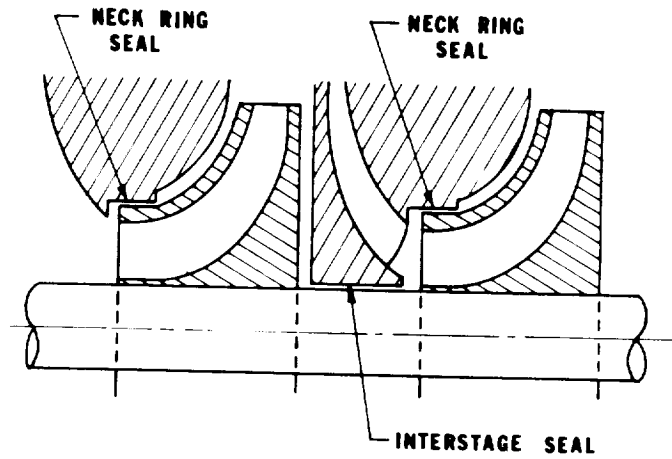


Figure 1. Seals in multistage centrifugal pumps

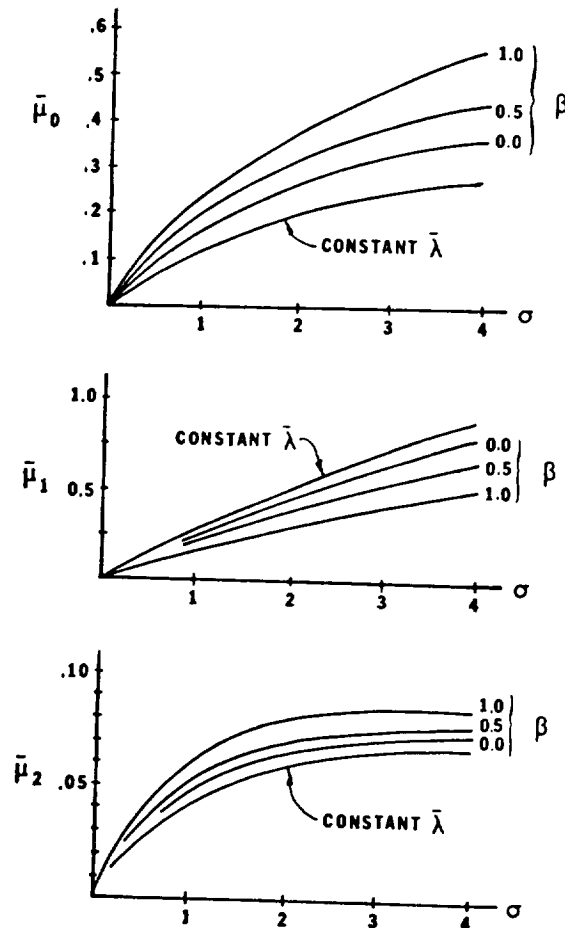


Figure 2. Dimensionless dynamic seal coefficients $\bar{\mu}_0$, $\bar{\mu}_1$, $\bar{\mu}_2$ versus σ and β for $\xi = 0.5$

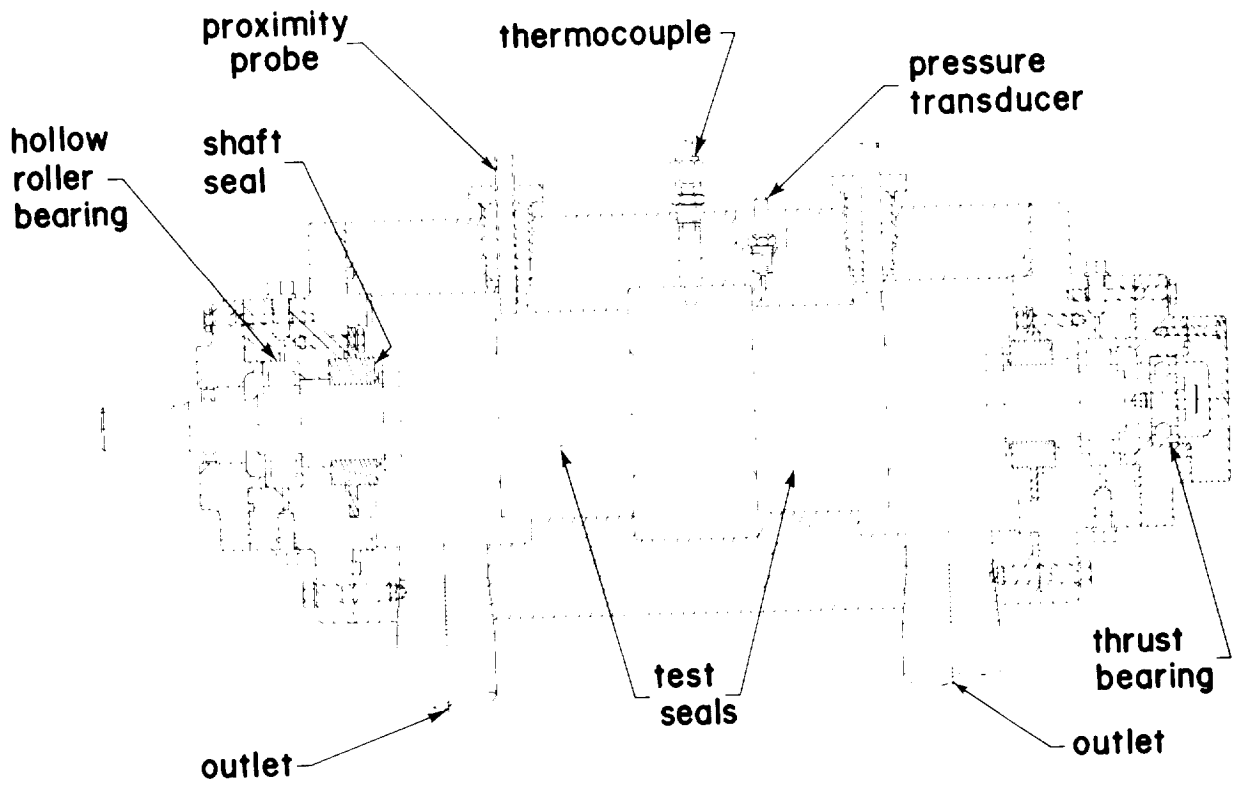


Figure 3. University of Louisville test section assembly

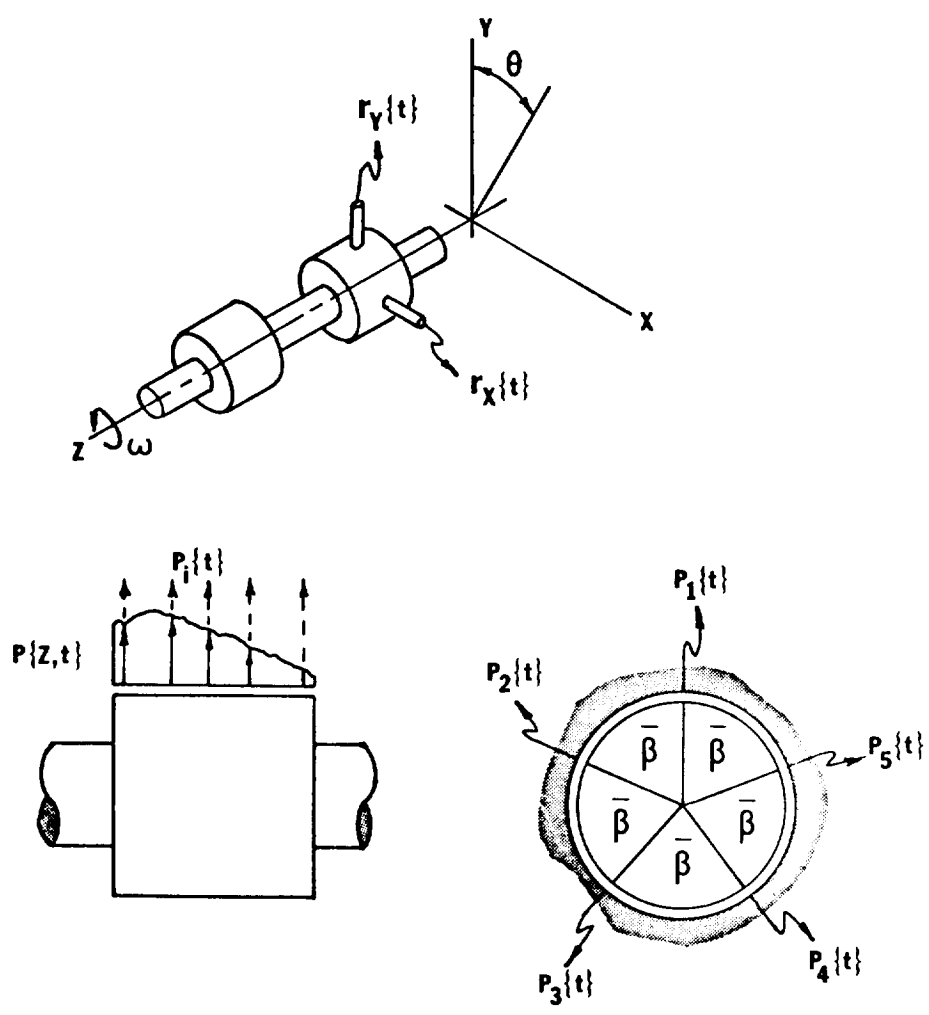


Figure 4. Instrumentation for the University of Louisville dynamic-seal test program

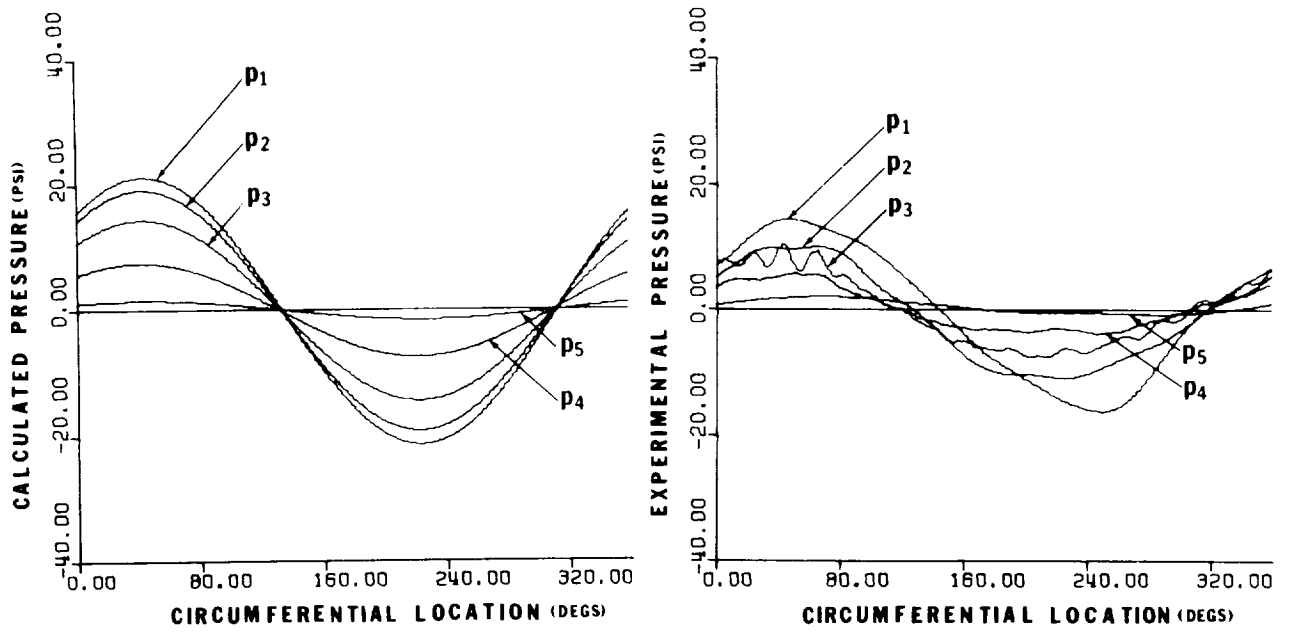


Figure 5. Theoretical and experimental pressure distributions for case 1 of Table 2

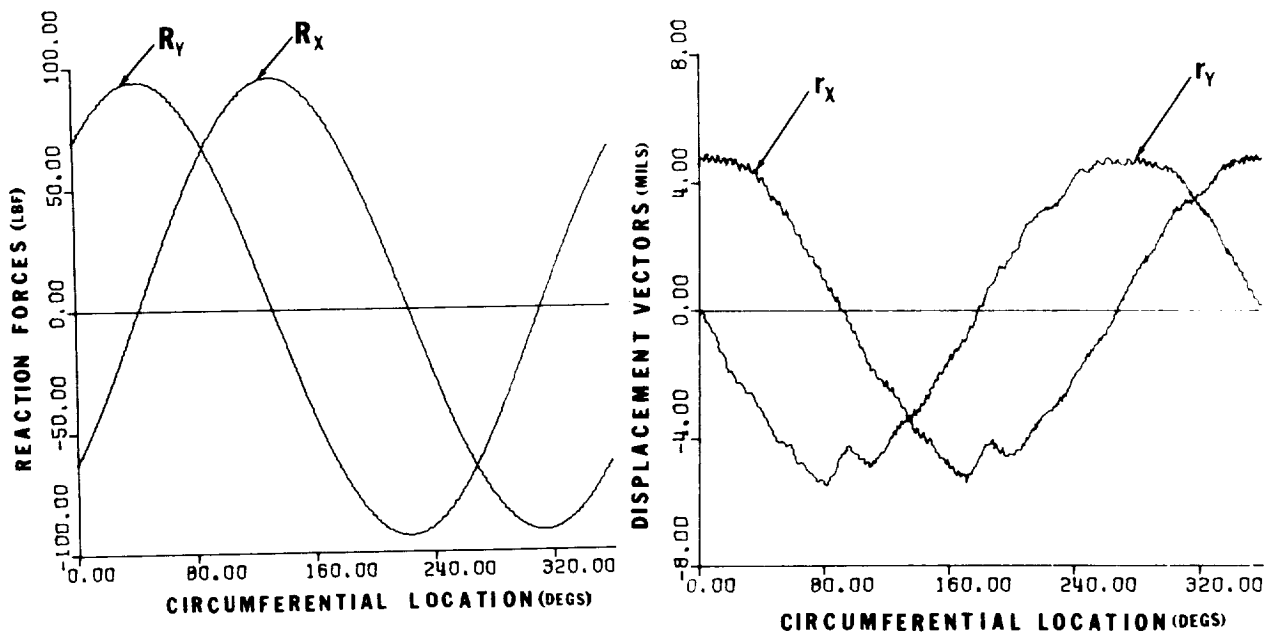


Figure 6. Measured reaction force and displacement components